International Journal of Disaster Risk Reduction 131 (2025) 105917

Contents lists available at ScienceDirect

International Journal of Disaster Risk Reduction

journal homepage: www.elsevier.com/locate/ijdrr

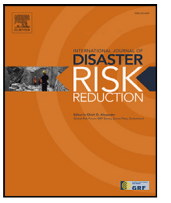

Including dynamics in a network-based stochastic multihazard model: A virtual testbed for volcanic ashfall and flood risk assessment☆

Mark Bebbington [a,*], Alexandre Dunant [b], David Harte [c], Stuart Mead [a], Melody Whitehead [a]

[a] Volcanic Risk Solutions, Massey University, Private Bag 11222, Palmerston North 4442, New Zealand
[b] EURAC, Viale Druso Drususallee, 1, 39100 Bolzano, Autonome Provinz Bozen - Südtirol, Italy
[c] Statistics Research Associates, 8 Bristol Street, Island Bay, Wellington 6023, New Zealand

ARTICLE INFO

Keywords:
Multihazard
Cascade
Network
Discrete-event simulation
Volcanic ashfall
Flood risk
Disaster Risk Management (DRM)

ABSTRACT

Network models have been previously proposed for spatial cascades of natural hazard events. These have generally not taken time into account, with the cascade of events effectively assumed to occur instantaneously. This study introduces a dynamic, network-based stochastic model developed as a virtual testbed to simulate complex multihazard interactions between multiple temporal processes, often occurring on different time scales. Since state of the art physical models generally involve heavy computation, the use of computationally simple probability distributions to describe the dynamics and interaction of the hazard events enables a larger number of model simulations, promoting greater robustness of model forecasts. The network modelling approach aims to allow the identification of key elements of the system that are most vulnerable, develop risk mitigation strategies, and examine restoration plans. We exemplify our methodology by investigating impacts of volcanic ashfall on river flow dynamics in the Rangitaiki and Tarawera river systems in New Zealand, simulating hydrological processes over a 365-day period with a volcanic eruption. Our results demonstrate how testbeds can be use to explore "what-if" cascading impacts scenarios, by providing a flexible, computationally efficient framework, offering crucial support for Disaster Risk Management (DRM) in volcanic regions.

1. Introduction

Understanding the complex interactions between multiple natural hazards remains one of the significant challenges in Disaster Risk Management (DRM). What will happen when multiple hazards strike? When, where, what and how large — these are the primary questions in assessing risk from natural hazards. However, the inherent complexity and interdependencies of natural hazards render the answers elusive [1]. Many large-scale disasters involve multiple hazards striking the same region either simultaneously, or before complete recovery from the first hazard's impact [2,3]. Multihazards are the occurrence of multiple hazards partially or completely overlapping in space–time that may or may not be causally related. Multihazards in which an initial event triggers a sequence of subsequent hazards create cascading impacts and complex risks that are difficult to predict and manage [1]. Examples

☆ This article is part of a Special issue entitled: 'Virtual Testbeds for DRM and CCA' published in International Journal of Disaster Risk Reduction.

* Corresponding author.
E-mail addresses: m.bebbington@massey.ac.nz (M. Bebbington), alexandre.dunant@eurac.edu (A. Dunant), david@statsresearch.co.nz (D. Harte), s.mead@massey.ac.nz (S. Mead), m.whitehead@massey.ac.nz (M. Whitehead).

https://doi.org/10.1016/j.ijdrr.2025.105917
Received 25 August 2025; Received in revised form 9 November 2025; Accepted 17 November 2025
Available online 18 November 2025

of cascading multihazards include volcanic ash fall during rain events [4], liquefaction or flood following earthquakes [5,6], or a landslide into a lake generating a tsunami [7].

To address this challenge, the scientific community is moving towards the development of virtual testbeds within a comprehensive digital ecosystem. Such testbeds aim to simulate complex multi-risk processes in realistic virtual environments, serving as laboratories for improving the understanding of cascading impacts and for testing mitigation and adaptation strategies through "what-if" scenarios. This paper contributes to the conceptualization and implementation of such a testbed.

Volcanic regions are prime examples of complex multihazard environments. Historical eruptions demonstrate the potential for widespread impacts extending far beyond the immediate vicinity of the volcano. For example, the 1314 Kaharoa eruption [8] over a 4–5 year period deposited at least 7.3 km^3 (Dense Rock Equivalent) of tephra, and created a dam at the outlet of Lake Tarawera that was subsequently breached [9]. Such widespread ashfall has the potential to trigger cascading hazards by interacting with other natural processes, most notably the hydrological cycle. A critical knowledge gap remains in our understanding of the dynamic interactions between volcanic ashfall and hydrological systems, which can lead to catastrophic compound events [10,11].

Models of individual natural hazards (e.g., floods, or volcanic ash deposition) are built from a combination of physio-chemical, numerical, and empirical relationships, the latter of which rely heavily on hazard-specific data [12]. Multihazard models have yet to reach a similar level of sophistication [13–15]. For example, an earthquake can create thousands of landslides and landslide dams, that themselves cause potentially disastrous outburst floods, such as have been recently observed in New Zealand during the 2016 Kaikoura earthquake [16–18]. Similarly, if an eruption is low-level but long-lived, persistent input of tephra to the system may cause a build-up of sediment in a reservoir and eventually cause frequent large-scale flooding [19].

There are two major hurdles impeding the development of robust multihazard models: the lack of data, and understanding the temporal dynamics of these complex hazard interactions. Multihazard data are required to build multihazard models, informing hazard occurrence, magnitudes, and subsequent inference as to potential hazard interactions [20]. However, while much conceptual work has been done around the generalization of multihazard interactions [21,22], there is a substantial lack of data to support any statistical analyses or formal quantification of these relationships. This fundamental gap may be partially filled by the simulation of potential multihazard *systems*.

Previous research has advanced the conceptual understanding of multihazard interactions [21,23], but often lacked the dynamic temporal elements required for realistic simulation. One proposed solution to quantifying the complexity in risk systems is to abstractly represent hazards and their interactions by networks [24,25]. However, the method is currently static, capturing end-member states, but without the ability to capture the evolving nature of cascading processes. To address these limitations, we propose a novel dynamic network-based stochastic multihazard model designed as a virtual parameterized testbed. Our approach incorporates temporal characteristics such as delays between event occurrences simulated using non-homogeneous Poisson processes into a spatio-temporal multi-risk framework, allowing for the realistic simulation of cascading events over time. By combining computationally efficient models for individual hazards and their interactions, we enable robust stochastic simulation over extended periods, providing a powerful tool for risk assessment and decision support.

Our model is applied to the Rangitaiki and Tarawera river systems in the Bay of Plenty region of New Zealand's North Island. Besides hosting the Okataina volcanic complex which has produced multiple large and long-lived eruptions during the Holocene [26], the area has the potential for ex-tropical cyclones [27], has multiple man-made dams providing scope for mitigation/management decisions, and was the location of the 1987 M6.5 Edgecumbe earthquake [28], that had well-documented effects on the Rangitaiki river [29]. Besides the dams, major infrastructure (Fig. 1) include the Edgecumbe GXP, the Te Ahi O Maui Geothermal Plant, pulp and paper mills, and the towns of Edgecumbe and Kawerau, located on the Rangitaiki and Tarawera rivers respectively. Network vulnerabilities arise at road and rail bridges, which carry on their underside communications and water pipes. The area is relatively flat, with the rivers contained by stop banks. These stopbanks represent both a threat to the bridges, through forestry debris, if they hold in a flooding situation, and to other infrastructure if they fail. Previous studies have quantified the effects of ash on dairy farms [30] and forestry [31], which represent the major land uses in the region (Fig. 2).

The remainder of the paper is organized as follows: In Section 2 we outline the network model and its relationship to Graph Theory, then link these concepts to a general set of natural hazards. This is followed in Section 3 by the hazard models that form the building blocks of a simplified version of the model, focussing on the details of a case study example of volcanic ash and precipitation applied to our case study of the Rangitaiki and Tarawera river systems. The results of the case study are presented in Section 4, and the methodology discussed in Section 5 along with suggestions on additional hazard modules to fill out the concept described in Section 2.

2. Network models for interacting multihazards

Dunant et al. [25] proposed a conceptual model of multihazard interactions and impacts using graph theory concepts. Hazards and infrastructure were assigned as nodes, and hazards that could trigger another hazard were linked, as were hazards and the particular infrastructure locations they could impact. The intent was to create an emergency-management focussed scenario generator for the extent of overlapping hazard impacts. The initial case study [25] was the M_w7.8 2016 Kaikoura (New Zealand) earthquake, in particular the roading network, which was severely impacted by coseismic and rain-triggered landslides. This was extended by Dunant et al. [13] to the area around Franz Josef (New Zealand), with the inclusion of landslide dams, flooding, stopbanks and buildings. Events in the multihazard cascade were made probabilistic, with landslide runout and inundation model outputs being included, and fragility functions for buildings, roads and stopbanks included to allow the results to be presented in the form of monetary loss.

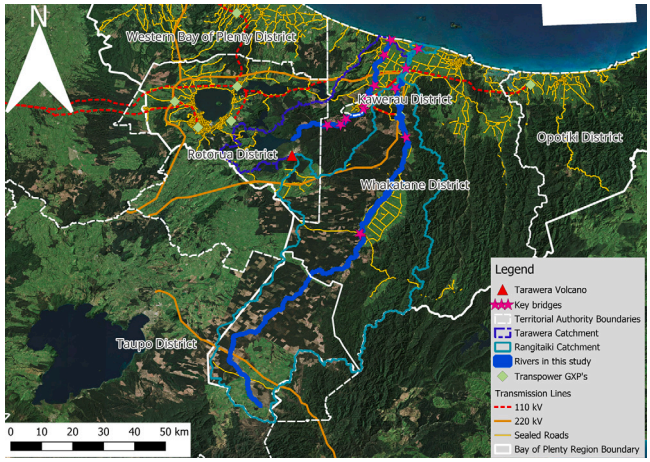

Fig. 1. The Tarawera and Rangitaiki catchments, road and power transmission networks [32].

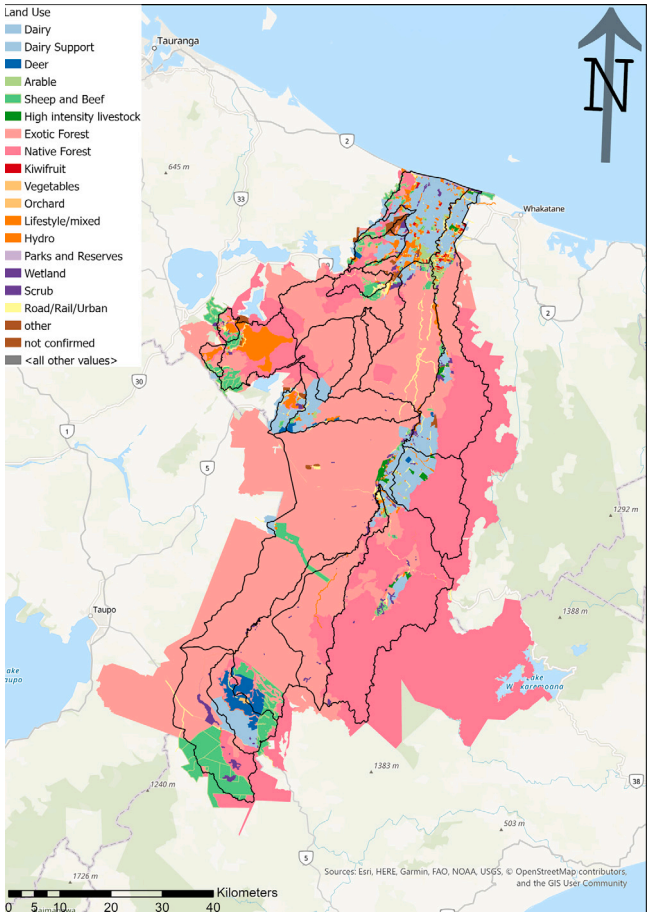

Fig. 2. Land use in the Rangitaiki-Tarawera catchment [32].

However, Dunant et al. [25] and Dunant et al. [13] accepted certain limitations. Most significantly, time was not included in either model. All connections were assumed to activate instantaneously, and downstream probabilities were not linked to the intensity of the upstream hazard. This paper presents a conceptual workflow with probabilistic, process-driven hazard models to overcome these limitations.

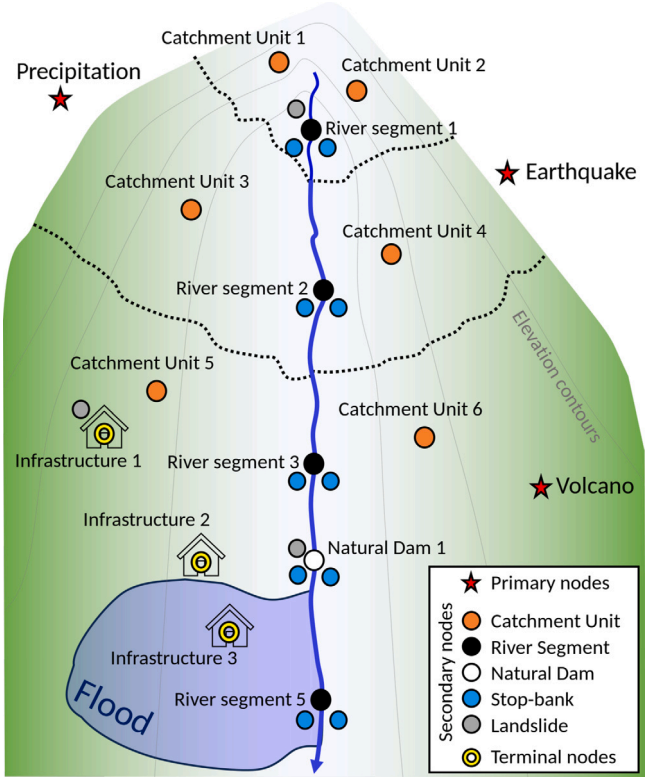

Fig. 3. Node locations in a virtual catchment. Various catchment units, separated by the black dashed lines, drain into the river (blue line) flowing down the valley. While the Landslide and Natural Dam nodes could occur at many random locations, in our application we only consider locations 'that matter', so they are pre-determined. The blue area represents a flood plain. Note that Natural Dam 1 is superimposed on River Segment 4. Primary nodes Precipitation and Earthquake are notionally placed outside the catchment, as their effects are applied uniformly throughout the catchment.

We think of a *network* as a system that is synonymous with graph theory [33]. As explained by Boccara [34, p.325–369], "A graph G is an ordered pair of disjoint sets (V, E), where V is a set of elements called vertices, *nodes*, or points, and a subset E of ordered pairs of distinct elements of V, called directed edges, arcs, or links". Thus, networks or graphs are objects composed of multiple components (*nodes*) and their interactions via links or ties (also known as *edges*). A network with directional edges is often called a *directed graph* or *digraph*. These graphs allow us to deal with several issues of complex systems by understanding the causality between the network components [35,36]. Explicitly incorporating temporal dynamics brings additional complications. For example, floods caused by stopbank failure are initially caused by heavy rainfall. But this is not an instantaneous process, it is time-modulated by lags; first there is excess rainfall runoff into the river, then river height increases, and then there is some further delay until the stopbank fails. Such processes, operating on multiple time scales, are not amenable to having time treated via a purely spatial network whose connections change at given points in time [37].

Since there are temporal processes operating at multiple time-scales (e.g. drainage of runoff water and deeply absorbed ground water), rather than adding the time dimension as a 3rd network dimension to the 2D spatial network, we treat time explicitly through discrete event simulation. Hence, the links and thus the network structure do not change over time, in contrast to the model considered by Holme and Saramäki [37]. Instead, the probability of propagation along an edge, the effects of such propagation and, most crucially, the delay in propagation varies with time, in a manner driven by the history of the process, which we describe as a *dynamic temporal spatial network*. In this section we will develop this new concept for the purpose of multihazard forecasting.

2.1. Virtual network design

The conceptual model consists of a virtual catchment (Fig. 3), susceptible to three major hazards: volcanic eruptions, precipitation, and earthquakes, with processes and likelihoods informed by the study area catchment of the Tarawera/Rangitaiki river systems. The simulation model consists of a nested temporal network that utilizes the phenomenological ideas behind a library of previously published stochastic and numerical models of processes and their triggering (described below).

We are modelling the effect of multiple physical processes and their interactions, which operate in continuous space and continuous time. We want to approximate this by selecting discrete locations in space (nodes) and the relationships between them

(edges), e.g., the virtual catchment shown in Fig. 3. Generally, our model nodes will represent a region (not a point) with a non-zero area and approximately homogeneous characteristics.

The way we define the spatial nodes and their physical extent (i.e., which nodes are physically adjacent to which) implicitly defines the connections (edges). Furthermore, our discrete nodes implicitly abstract spatial relationships to some degree. This abstraction results in a trade-off between bias and variance: finer detail (more nodes), and you get more precision but possibly miss certain rare events due to the decreased number of repetitions due to computational cost. This is particularly fraught in natural hazard applications, where it is precisely these rare events that we struggle to quantify.

Therefore, the nodes must be defined with the objective of the exercise firmly in mind [38]. The model needs to reflect the known behaviour of the system [39] as well as the end-user aspirations. Further, the model must be guided by thoroughly quantified output, computing limitations, and a comprehensible way to convey the results. By defining a judicious set of nodes, some underlying processes will not be explicitly included in the model as they would add too much complexity; for example, internal processes of gravity mass movement or fault network structure underlying the earthquake behaviour [40,41]. Such detail would not be useful for the final purpose of the method. Our chosen approach to determining the right hierarchical scale of the analysis is to consider only those physical effects that are directly observable (e.g., shaking, mass movement, water depth).

It is stressed that a conceptualization is needed whereby the objects of the system are drawn as points (nodes). Our method assumes that an area of interest (AOI) can be considered as a disaster macrosystem composed of *hazard nodes* (or sources, e.g., earthquake, river, slope unit) and *exposed nodes* (e.g., houses, roads). Hence a *node* could represent a fault segment, a contributing source area of landslides, a storm, a river, a road segment, a house, or any other "entity" depending on the specific purpose of the exercise and the natural hazards characteristic of the AOI. The various nodes are considered separate entities with their specific spatial patterns and behaviours. They relate to each other by specific rules based on empirical data, mathematical models, and expert opinion.

2.2. Node types and triggers

We define three node types in our conceptual model: Primary, Secondary and Terminal, where the following rules apply.

1. An event on a Primary node initiates a cascading process by triggering events on Secondary and/or Terminal node(s).
2. An event on a Secondary node can continue the cascade by triggering events on another Secondary node(s) and/or Terminal node(s), but cannot trigger an event on a Primary node.
3. An event on a Terminal node can be triggered by an event on a Primary or Secondary node, but the Terminal node cannot trigger any subsequent event, a specific sequence terminates here.

In our application, the Primary nodes considered are: Volcano, Precipitation and Earthquake; Secondary nodes considered are: Catchment Unit, River Segment/Man-made Dam, Landslide, Stop-bank, and Natural Dam; and Terminal nodes are Infrastructure of varying types. We define a Catchment Unit as a contiguous area with similar overall slope that drains to a single River Segment/Man-made Dam. A man-made dam is treated as a River Segment, with different (controllable) flow dynamics.

The network is operating in a semi-closed system within a Network Pseudo Boundary (NPB) where only Primary nodes can initiate a sequence of events within the NPB; see Fig. 4. Clearly the Primary nodes must be triggered by something, but this triggering, possibly part of a wider external network, is not within the NPB. In this sense the network of interest is semi-closed or pseudo, and the Primary nodes can be thought of as self triggering in a computer simulation of events on the network. In theory the methodology can extend to secondary nodes triggering themselves, but this is not the case in the example presented herein.

2.3. Simulation with varying time lags

We provide a discrete-event simulation [42] algorithm for simulating events on a dynamic temporal network, i.e. where there is a time delay (lag) between the occurrence time of the triggering event and the triggered event. This time lag may vary according to the 'history' of the process, and so could even be different between the same trigger and triggered nodes at a different time in the sequence because of a different past history. The temporal delay is described as a non-homogeneous Poisson process, simulated by the Point process thinning method [43,44], which has been applied to multi-hazards [45]. The algorithm to simulate events in the time interval $(0, T)$ is given in Table 1, using the notation in Fig. 4.

The simulation algorithm is constructed in such a way that when real time is equal to the activation time t of the ℓth triggered Secondary event in step 6, we know the complete history of the process up until time t. Thus we know all input parameters of an event at its time of activation, at which point, the algorithm simulates all later events that the just-activated event triggers. Given our knowledge of the history up until t, the algorithm can pass on characteristics of the triggering event (just-activated) to all of its triggered events. For example, a large activated event could be made to induce a larger effect on its triggered events. This complete history also allows one to re-evaluate the activated node's 'vulnerability' or response to future triggers which may change during the cascade sequence. This includes the potential for multiple past triggers, each occurring with a different time lag.

In Table 2, the source is the hazard triggering node which affects its listed target nodes *without intermediate nodes*, hence there is a *directed edge* from a source node (trigger) to each of its listed target nodes (triggered). Secondary nodes can also trigger effects on other secondary and terminal nodes, but not on the primary nodes. A graphical representation of the node structure discussed above, and the directed links (edges) between the nodes is shown in Fig. 5.

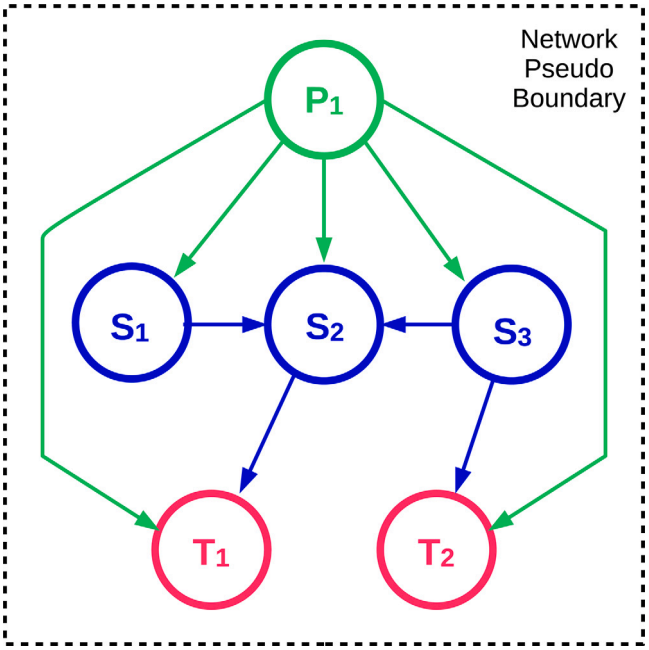

Fig. 4. A hypothetical example. The arrows represent *directed edges*. The process is initiated by the Primary node P_1 (green), and can trigger Secondary (blue) and Terminal (red) nodes. The Secondary nodes can trigger other nodes within the NPB (excluding Primary), and the Terminal nodes cannot trigger. The depicted network and NPB are *not necessarily spatial*, it is about the *relationship between the nodes, i.e. all edges are directed to nodes within the NPB.*

Table 1
Simulation algorithm for events in the time interval $(0, T)$. Note that the 'history' of the simulated process is complete up to t in step 5 (i.e. ℓth triggered Secondary event) because no events can be simulated before t in step 5; i.e. we have full past knowledge of the process up to t. Further, because of potentially very different lag times between the occurrence time of a triggering event and its triggered events, the events are not necessarily simulated in chronological order in step 6. This is why it is important to re-sort after each simulation (step 6). Clearly many more system variable values, describing the state of the network at time t, could be saved at step 6 of the algorithm.

Simulation Algorithm	
1	We create an event list where each record represents an event, with variables: `triggering.node.name`, `triggered.node.name`, and `activation.time`; plus any other sequence specific variable values required during the simulation.
2	Simulate times of all events in $(0, T)$ on all p primary nodes P_i, where $i = 1, \ldots, p$. For each event, record the node name (P_i) and its activation time $t \in (0, T)$. Add each record to the event list. In this special case, the node name goes into the `triggered.node.name` column, and the `triggering.node.name` is blank. All events in $(0, T)$ on Primary nodes can be simulated at this stage because, by assumption in Section 2.2, there is no feedback from within the NPB, i.e., they are independent of the 'history' of the process.
3	For each event simulated on a Primary node, simulate all events it triggers on Secondary nodes $(S_j, j = 1, \ldots, s)$ and Terminal nodes $(T_k, k = 1, \ldots, \tau)$. For each simulated event, record the triggering Primary node name (P_i), the triggered node name (S_j or T_k), and its activation time t. Add each record to the event list. *Sort the updated event list by activation time.*
4	$\ell \leftarrow 1$.
5	Return to the ℓth *triggered* Secondary event in the event list. If $t > T$, where t is the time of this event, go to step 9, there are no further events in $(0, T)$; else continue.
6	Simulate all events that the ℓth *triggered* Secondary event subsequently triggers on Secondary nodes $(S_j, j = 1, \ldots, s)$ and Terminal nodes $(T_k, k = 1, \ldots, \tau)$. For each simulated event, record the triggering node name, the triggered node name (S_j or T_k), and its activation time t. Add each record to the event list. *Sort the updated event list by activation time.*
7	If no additional events were simulated at step 6 and the ℓth triggered Secondary event is the last triggered Secondary event in the list, go to step 9, the cascade is complete.
8	$\ell \leftarrow \ell + 1$, then go to step 5.
9	Delete events from the list where $t > T$.

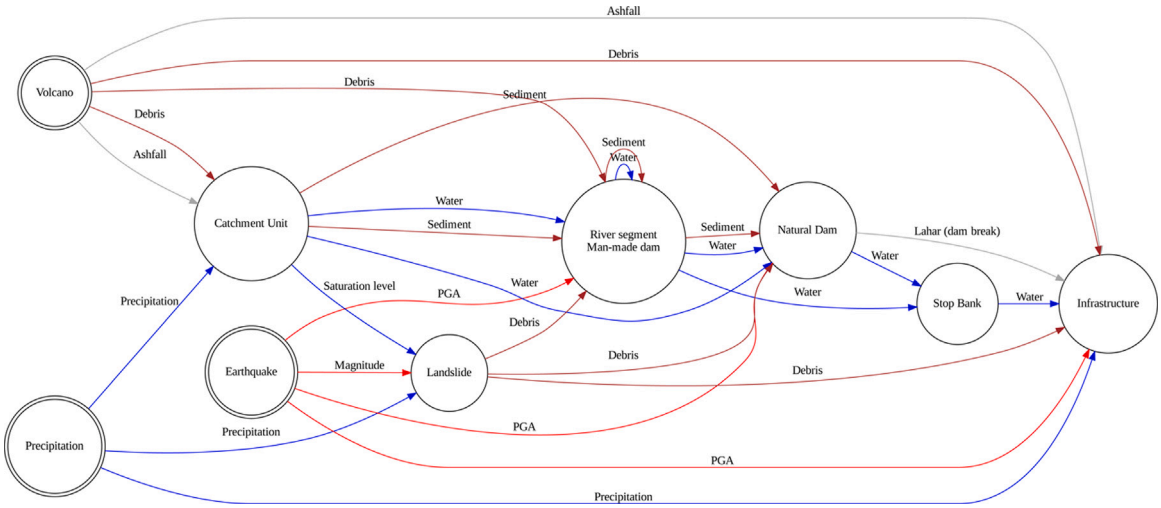

Fig. 5. Connections (edges) between nodes within the multihazard system. The double circles represent *Primary nodes*, node and edge descriptions are found in Section 2.2.

Table 2
Hazard triggering pairs (directed edges).

Source	Process	Target[a]	Mark
VOLCANO (V)	Ashfall	CU	Volume
	Debris flow	CU	Volume
	Debris flow	RS	Forms ND
	Ashfall	INF	Impact (fragility functions)
	Debris flow	INF	Destroyed
PRECIPITATION (P)	Rainfall	CU	Rainfall/time
	Rainfall	LS	Rainfall/time
	Rainfall	INF	Impact (fragility functions)
EARTHQUAKE (E)	Shaking	LS	Landslide triggering
	Shaking	RS	Dam failure triggering
	Shaking	ND	Dam failure triggering
	Shaking	INF	Impact (fragility functions)
CATCHMENT UNIT (CU)	Rainfall run-off	RS	Volume
	Sediment run-off	RS	Volume
	Rainfall run-off	ND	Volume
	Sediment run-off	ND	Volume
	Saturation	LS	Proportion
RIVER SEGMENT/	Streamflow	RS[b]	Discharge volume
MAN-MADE DAM (RS)	Sediment transfer	RS[b]	Sediment load/bed level
	Streamflow	ND[b]	Discharge volume
	Sediment transfer	ND[b]	Sediment load/bed level
	Streamflow	SB[c]	Flow level
STOP BANK (SB)	Failure	INF	Flooded
NATURAL DAM (ND)	Overflow	RS	Dam forms a weir
	Dam collapse	INF	Lahar destroys all nodes downstream including SB
LANDSLIDE (LS)	Landslide	RS	Forms ND
	Landslide	ND	Reinforces ND
	Landslide	INF	Destroyed if runout reaches node
INFRASTRUCTURE (INF)	N/A	N/A	N/A

[a] Primary, Secondary and Terminal nodes are denoted by one-, two- and three-letter codes, respectively.
[b] Downstream only.
[c] One on each side of the river segment.

3. Virtual testbed

The modelling of multiple hazard processes becomes extremely complex for at least two reasons: state of the art physical models for each individual hazard process can have very high computational requirements (e.g. weather forecasting) and a high number of parameters [46]. Secondly, it is not clear how to deal with the overall aleatoric uncertainty with multiple interacting hazards. Hence, in the graph model presented herein, the simulation requires known empirical relationships, with considerably less computational

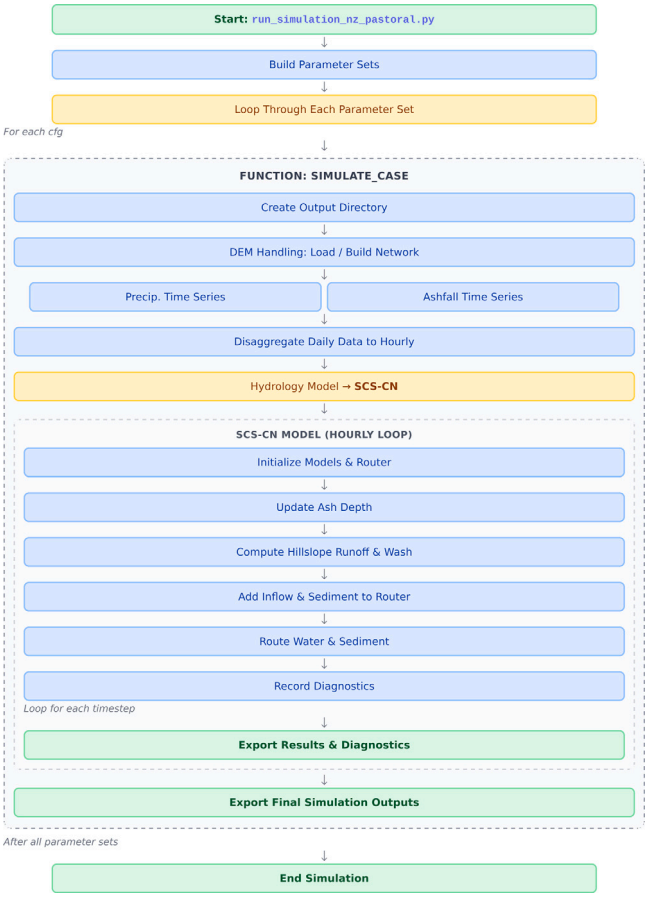

Fig. 6. Algorithm flowchart.

effort [47], and effectively accounting for the aleatory (stochastic) uncertainty. In the case study presented herein we illustrate a restricted subset of the model containing the ashfall/precipitation/streamflow interactions, and then later discuss how additional processes can be added into the model. The equations of the processes described in the subsequent section, and use in the case study, can be found in the Appendix of this paper. The virtual testbed is built upon a modular framework where each component simulates a specific physical process on an hourly time step. The overall architecture is designed to capture the cascading effects from volcanic ash deposition to altered hydrological response and subsequent sediment transport. An overview of the algorithm is summarized in Fig. 6.

The study area, including the delineated catchments and the network model structure consisting of nodes (reaches) and edges (connections), is shown in Fig. 7. The volcanic source for ashfall simulations was Mt Tarawera in the Okataina caldera. It is important to note, in the context of a testbed herein, that any Digital Elevation Model and volcano location can be used, allowing for application to different geomorphological settings.

3.1. Stochastic precipitation model

The model is driven by a stochastic precipitation generator that produces daily rainfall data, which is subsequently disaggregated to an hourly timescale. Daily rainfall depth (z, in mm) is drawn from a Gamma distribution to account for the skewed nature of precipitation events:

$$z = \Gamma\left(\alpha, \frac{\mathrm{MAP}}{\alpha}\right). \tag{1}$$

The shape parameter α for this distribution is controlled, in the context of a modular test bed, by a user-configurable value, and scaled by mean annual precipitation (MAP), measured in mm. Intermittency of rainfall (i.e. the chance of a dry day) is governed by a rain probability parameter P_{rain}, with seasonal patterns defined as a sinusoidal function scaled by a strength parameter S_{season} to modulate the daily rainfall totals for every day (d_i) of the year as:

$$\boldsymbol{R_i} = z\left(S_{\mathrm{season}} \sin\left(\frac{2\pi d_i}{365}\right) + 1\right) P_{\mathrm{rain}}. \tag{2}$$

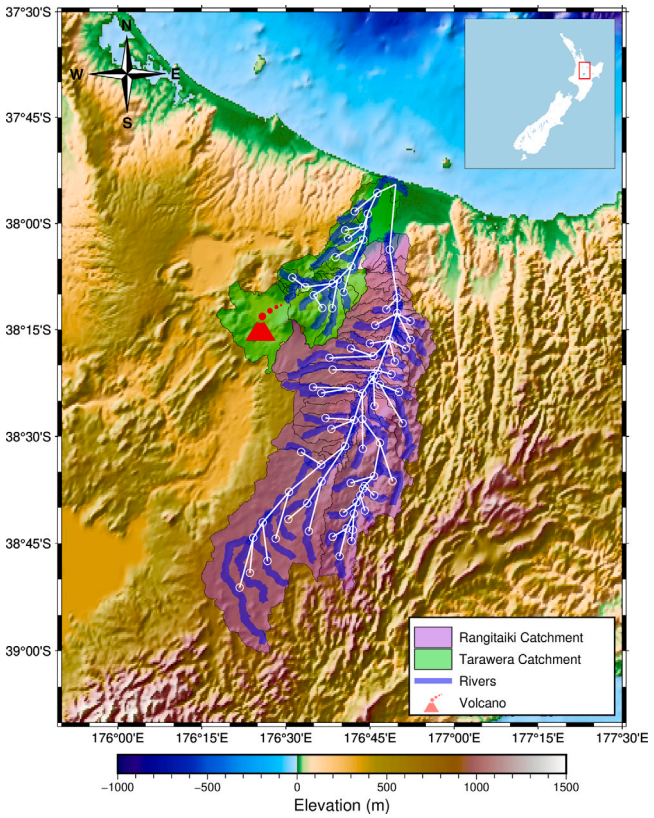

Fig. 7. Map of the study area showing the Rangitaiki and Tarawera river systems in relation to the local topography and the Okataina caldera. The model's network structure, consisting of nodes (river reaches — white circles) and edges (downstream connections — white lines), is overlaid on the catchments. The location of the volcanic source for ashfall simulations is also indicated.

Finally, the daily precipitation is uniformly disaggregated into hourly values $r_i = R_i/24$ within the hydrology model. This simplification ensures consistency with the (sub)model's hourly timestep and reflects the study's focus on catchment-scale cumulative responses rather than short-duration convective rainfall events. Future developments of the framework could incorporate higher-resolution rainfall forcing when required for applications where sub-daily rainfall variability becomes crucial.

3.2. Volcanic ashfall simulation

Intermittent volcanic eruptions, which act as the primary trigger for the cascading hazard sequence, are simulated using a flexible stochastic framework. The model offers two distinct modes for determining the timing of eruptive events: a *Stochastic Renewal Process* for long-term probabilistic assessment using a Weibull distribution [48], and a *Deterministic Scenario* that uses a predefined list of eruption days for "what-if" analyses.

When an eruption is triggered, its magnitude and dispersal characteristics are determined stochastically based on the tephra fall model of González-Mellado and De la Cruz-Reyna [49]. First, an erupted mass (M_0) is calculated, which then scales the parameters governing the ash dispersal. The resulting tephra thickness (in mm) at any point on the landscape is given as a function of the distance (d) and angle (θ) from the vent, an effective eruption size (γ_{eff}), a distance-decay exponent (α_{eff}), deposit elongation through diffusivity (β) and wind speed (U) and the dispersal axis (wind direction), (ϕ):

$$T(d,\theta) = \gamma_{\text{eff}} \cdot \exp[-\beta U d(1-\cos(\theta-\phi))] \cdot d^{-\alpha_{\text{eff}}}. \tag{3}$$

This parameter-driven approach allows the testbed to explore a wide range of potential volcanic activities and their cascading impacts. The full equations for estimating eruption magnitude and ash dispersal parameters $\gamma_{\text{eff}}, \alpha_{\text{eff}}, \phi$ and the product βU are detailed in Appendix.

Once the total ashfall depth for each catchment is calculated, it is uniformly disaggregated to an hourly rate, providing the necessary input for the time-step-based hydrological and sediment transport models.

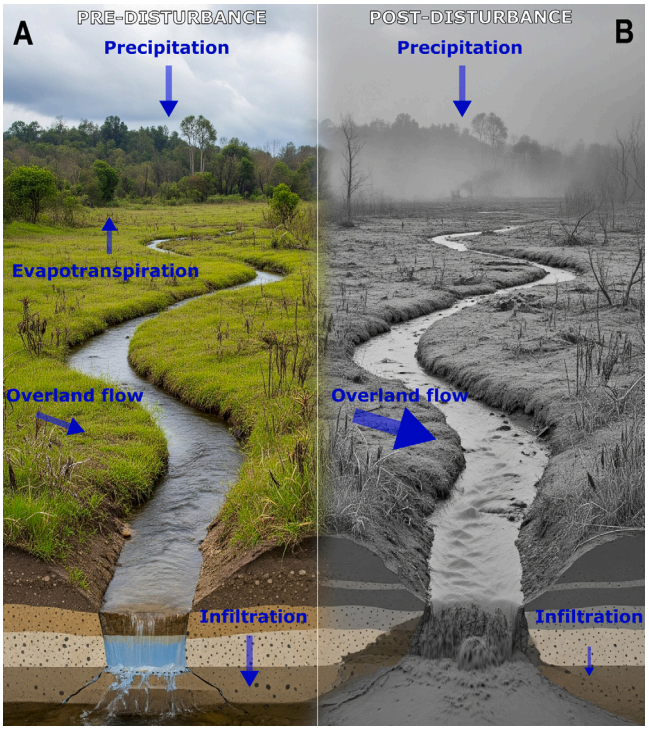

Fig. 8. Conceptual illustration of the primary cascading impact mechanism modelled. **(A)** In pre-disturbance conditions, precipitation is partitioned into interception, infiltration, and overland flow. **(B)** Following a volcanic eruption, a tephra-fall layer blankets the ground, sealing soil pores. This significantly reduces infiltration and increases the proportion of precipitation that becomes overland flow, leading to faster and larger flood peaks (modified from [51]).

3.3. Hydrological response and ash mobilization

The hydrological simulation translates precipitation and ashfall into river discharge and sediment flux. Runoff from each catchment is calculated using the Soil Conservation Service Curve Number (SCS-CN) method [50]. This widely-used, empirical model is well-suited for a virtual testbed due to its computational efficiency and because its central parameter, the Curve Number (CN), can be dynamically modified to represent changing landscape conditions. Here the key cascading impact of increased discharge and flood risk is driven by the physical sealing of the soil surface by ash, a process that is dynamically modelled.

The effective runoff depth (Q_{runoff}) from an hourly precipitation value (r_i, in mm) is given as

$$Q_{\text{runoff}} = \frac{(r_i - I_a)^2}{r_i - I_a + S_{\text{eff}}} \quad \text{for } r_i > I_a \tag{4}$$

where (I_a) is an 'initial abstraction value' that represents surface storage and initial infiltration (i.e. rainfall loss). The runoff calculation is moderated by the soil retention value (S_{eff}), governed by the effective curve number (CN_{eff}):

$$S_{\text{eff}} = \frac{1000}{\text{CN}_{\text{eff}}} - 10 \tag{5}$$

where CN_{eff} varies with ash thickness (T from Eq. (3)) and a decay constant (k_{ash}, see Appendix for full equations). This additional parameterization captures the dynamic impact of ashfall on runoff, not captured in traditional SCS-CN methods. As illustrated conceptually in Fig. 8, the ash layer seals soil pores, which significantly reduces infiltration and increases the fraction of rainfall that becomes surface runoff. This is represented by increasing the effective Curve Number (CN_{eff}).

Rather than a simple linear increase, the model implements a more physically realistic exponential saturation function. This function ensures the initial, thin layers of ash have the most pronounced effect on sealing the soil, with the impact diminishing as the ash layer thickens (see Appendix for formula). This non-linear approach is crucial for capturing the exaggerated flood response observed after eruptions.

Ash that has been deposited on the hillslopes is made available for transport by rainfall. The mass of ash washed into the river during one time step (M_{wash}) is limited by the total mass of ash available in the catchment (M_{avail}) and proportional to the efficiency of ash wash (η_{wash}) and runoff (Q_{runoff} from Eq. (4)):

$$M_{\text{wash}} = \min\left\{ M_{\text{avail}}, M_{\text{avail}} \cdot \eta_{\text{wash}} \cdot \left(\frac{Q_{\text{runoff}}}{\Delta Q_{\text{ref}}} \right) \right\}, \tag{6}$$

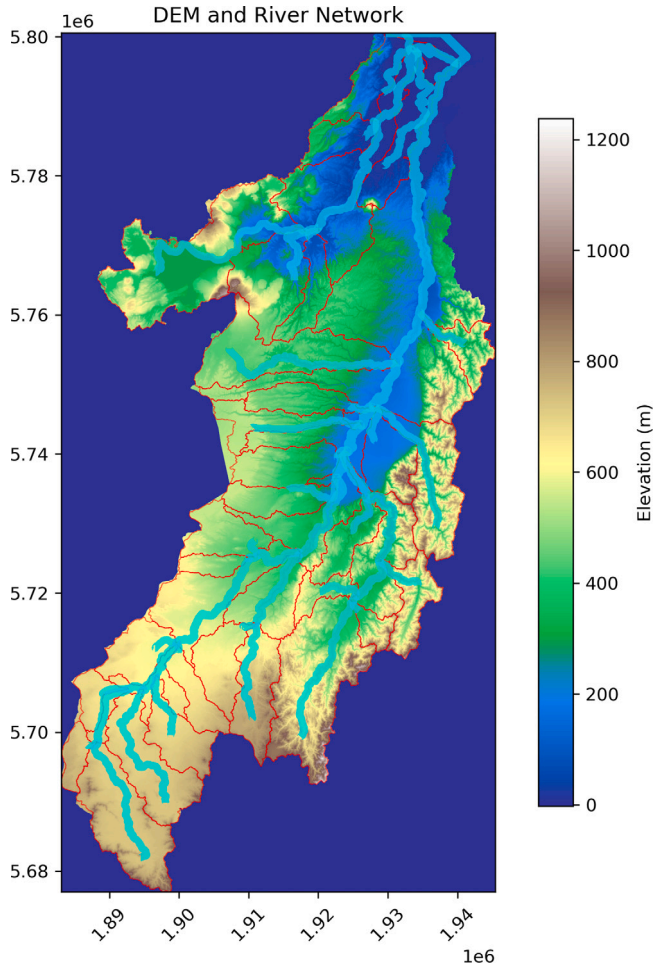

Fig. 9. Automated extraction of the river network and its characteristics from the input DEM and the delineated river reaches and sub-catchment boundaries overlaid on the Digital Elevation Model (DEM).

following the principles of the Universal Soil Loss Equation approach [52].

The hourly runoff volume from each catchment is converted into a discharge hydrograph by convolution with a triangular Unit Hydrograph (UH). The shape of the UH is determined by the catchment's time of concentration, t_c, which is calculated using the Giandotti formula based on catchment area, channel length, and elevation drop (see Appendix for all UH equations). The generated hydrographs are then routed through the river network using a lag-based system where travel time in each reach is a function of its length and a defined channel velocity.

Transport of ash washed into the river is governed by the hydraulic conditions in each reach. The transport capacity is based on bed shear stress, τ, which is calculated at each step based on the current discharge, channel slope, and channel geometry (see Appendix for transport equations). The mass of ash transported (T_c, in kg per timestep) is then calculated as a power-law function of this shear stress, scaled by the ash transport coefficient k_t, ensuring that sediment routing is highly responsive to the flow conditions:

$$T_c = k_t \cdot (\tau^{1.5}) \cdot W \cdot L, \tag{7}$$

where W and L are the channel width and length.

3.4. Simulation design

To clearly illustrate the model's capability to analyse cascading impacts, we designed a comparative "what-if" analysis centred around a significant volcanic eruption. A detailed simulation was conducted for a 365-day period on an hourly time step, using the `scscn` model configuration. This design allows the period prior to the eruption to serve as a baseline "no-ash" scenario, against which the post-eruption "ash-impacted" scenario can be directly compared. The key variables (from Eqs. (1) through (7) and the Appendix), and their parameterization for this case are shown in Table 3

Table 3
Parameters, variables and values for New Zealand North Island land-use scenario.

Parameter	Variable	Value
Precipitation		
α	precip_sigma	5.0
MAP (mm)	mean_annual_precip	2500
P_{rain}	rain_prob	0.5
S_{season}	season_strength	0.2
Ashfall		
γ_0	gamma0	0.0016
α_0	alpha0	794.0
M_0	M0	4.0
Runoff		
I_a	initial_abstraction_ratio	0.05
CN_{base}	curve_number	70
k_{ash}	k_ash	0.5
$\text{CN}_{\text{max\_increase}}$	max_cn_increase	25
η_{wash}	wash_efficiency	0.05
Hydrology		
k_t	transport_coefficient	5e−4
v	channel_velocity_ms	0.5

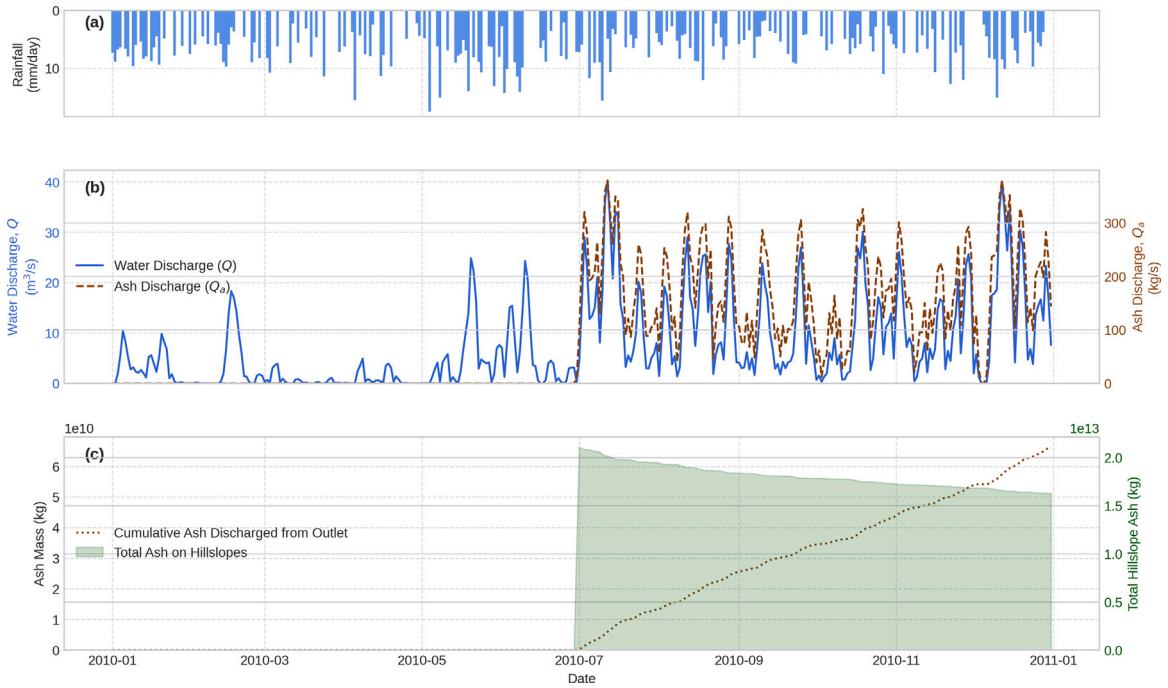

Fig. 10. Stock and flow relationship for the 365-day simulation with an eruption on day 180. **(a)** Daily rainfall driving the system. **(b)** Hydrograph (blue line) and ash discharge (brown dashed line) at the network outlet. **(c)** Ash stocks, showing the total mass of ash remaining on the hillslopes (green shaded area) and the cumulative mass of ash discharged from the network outlet (dotted line).

For this specific analysis, we opted for a deterministic eruption scenario. While the model is fully capable of simulating long-term hazard exposure using a stochastic Weibull distribution for inter-eruption timing, a single, predefined eruption on day 180 was chosen. This approach allows for a clear and unambiguous demonstration of the stock-and-flow dynamics and the direct hydro-sedimentological consequences of a single ashfall event without the confounding effects of multiple, randomly timed eruptions. The parameters were chosen to represent a typical pastoral land-use scenario in New Zealand's North Island.

4. Results

The simulation results provide a detailed picture of the dynamic, cascading interactions between volcanic ashfall, rainfall, and river system response. We focus on the stock-and-flow relationship, which describes how ash (stock) is stored in and released from the catchment and river network in response to hydrological events (flow).

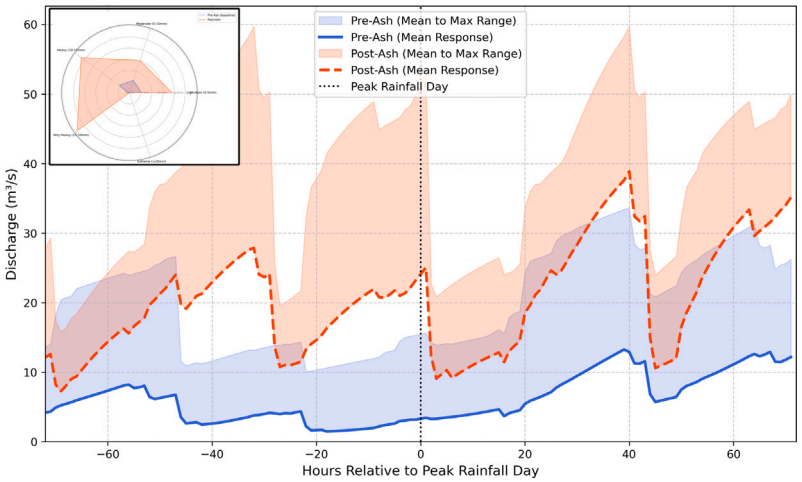

Fig. 11. Ensemble hydrograph response comparing isolated and aggregated hydrographs from multiple, distinct storm events before and after the ashfall event. The radar diagram in the upper left corner represent the river discharge overlap between ash and no ash periods for different precipitation bins.

4.1. Ash stock and flow dynamics

The foundation of the simulation is the river network itself, which is extracted automatically from the Digital Elevation Model (DEM) provided as an input. As shown in Fig. 9, the `pyflwdir` library processes the DEM to delineate catchment boundaries and derive a stream network based on a minimum threshold for the Horton-Strahler stream order [53], which was set to (≥ 8) for this study and can be updated in the simulation. The resulting network provides the spatial structure for routing water and sediment, making the analysis adaptable to any virtual testbed scenarios.

The 365-day simulation included a significant eruption event on day 180. Fig. 10, generated directly from the simulation outputs, presents the core results, illustrating the relationship between hydrological drivers, sediment flow, and sediment stocks.

Panel (a) of Fig. 10 shows the daily rainfall driving the system. Panel (b) illustrates the system's "flow" response at the outlet. Water discharge (blue line) responds rapidly to rainfall throughout the year. Ash discharge (brown dashed line), however, is contingent on the availability of ash (in this example, no ash discharge before day 180). Immediately following the eruption, rainfall events trigger significant ash discharge peaks in the river. This highlights the critical role of antecedent ashfall in mobilizing sediment.

Panel (c) visualizes the ash "stock" dynamics. The total mass of ash on hillslopes (green shaded area) appears instantly on day 180 and is subsequently depleted by rainfall-driven wash-off events. The cumulative ash discharged from the outlet (dotted line) rises in steps, with each step corresponding to a period of ash mobilization. The difference between the initial hillslope stock and the cumulative discharged mass represents the ash that is either still on the hillslopes or in storage within the river network itself.

To further quantify the impact of ash on hydrological response, Fig. 11 compares the ensemble of hydrographs from significant storm events ($>$ 10 mm/day) before and after the eruption. The script first identifies all significant storm events in the 365-day simulation period, defined as any day where the total rainfall exceeds a threshold of 10 mm/day. These storm events are then separated into two distinct ensembles based on their timing relative to the day 180 eruption: a "Pre-Ash" group and a "Post-Ash" group. For every storm in each ensemble, the corresponding hourly discharge hydrograph is extracted for a 144-hour window (72 h before and 72 h after the day of peak rainfall). All hydrographs within an ensemble are then aligned on a relative time axis, with time zero representing the peak rainfall day. The statistical properties of each ensemble are then calculated. For every hour on the relative time axis, it computes the mean and the maximum discharge across all hydrographs in the group. The plot shows the mean response (solid and dashed lines) and the range from mean to maximum response (shaded areas) for pre-ash (blue) and post-ash (orange) conditions, aligned to the day of peak rainfall. Each discharge peak corresponds to a discrete rainfall event exceeding 5 mm/day, separated by dry intervals, explaining the observed variability.

The resulting plot clearly demonstrates the cascading effect of ashfall. The post-ash hydrographs (orange) are significantly more variable. The mean response (dashed orange line) is consistently higher, and the range between the mean and maximum response (shaded orange area) is far larger than for the pre-ash events (blue). This illustrates that for a given amount of rainfall, the river system produces a faster and larger flood peak after being blanketed by ash. This is a direct consequence of the physical mechanism modelled: the ash layer seals the soil surface, reducing infiltration and converting a larger fraction of rainfall into rapid surface runoff, thereby dramatically increasing flood risk.

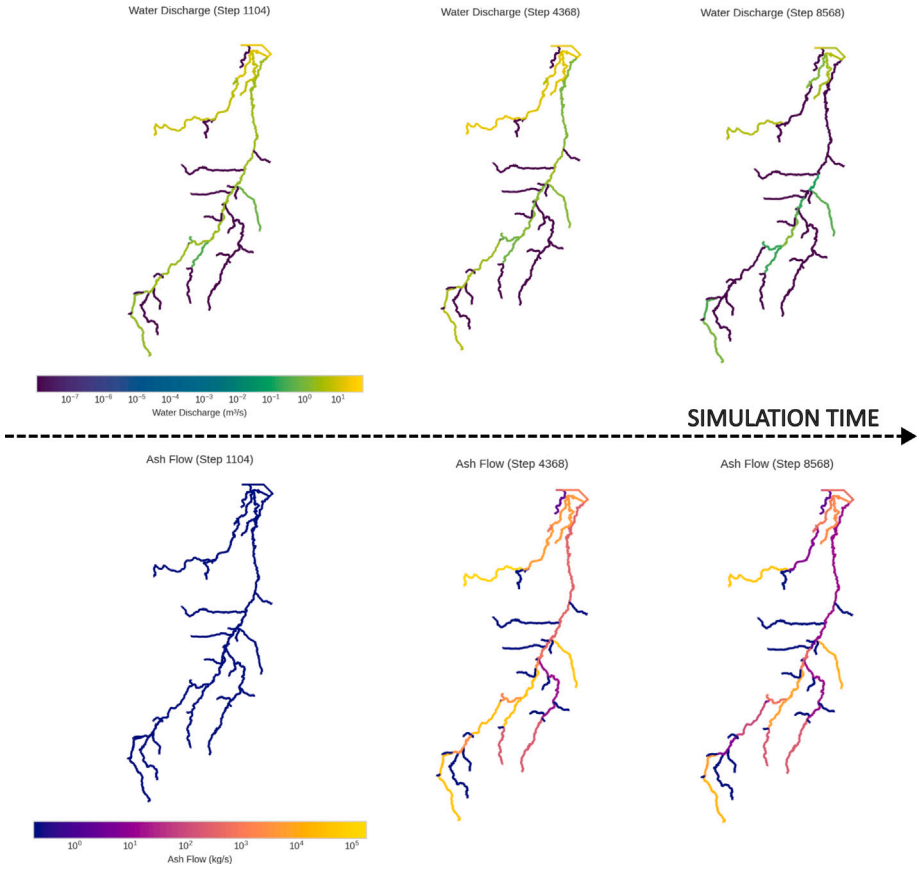

Fig. 12. Snapshots from the simulation showing the spatio-temporal evolution of water and ash flow through the river network. The top row displays water discharge (m^3/s) and the bottom row shows the corresponding ash flow (kg/s) at three key moments. **(Left, Step 1104/Day 46):** Baseline, pre-eruption conditions with normal water discharge and negligible ash flow. **(Center, Step 4368/Day 182):** The period immediately following the day 180 eruption, where a rainfall event is mobilizing fresh ash from the headwaters into the river system. **(Right, Step 8568/Day 357):** The long-term response, showing the ash pulse has propagated downstream and is now concentrated in the main stem of the river network, long after the initial event.

4.2. Spatio-temporal cascade dynamics

The virtual testbed also allows for visualization of the cascade's spatial evolution. Fig. 12 shows snapshots from the simulation, illustrating how water and ash propagate through the network at key moments.

Water discharge is a persistent feature of the network, present at all stages of the simulation (Fig. 12, top row). In contrast, significant ash flow is highly transient and localized (Fig. 12, bottom row), activated only where there is both available ash and sufficient water flow. The snapshots clearly illustrate the life cycle of the ash pulse. Initially, there is no ash in the system (left panel). Immediately after the eruption, the ash is mobilized in the headwater catchments where it first landed (centre panel). Weeks later, the pulse has been advected downstream and is now concentrated as a wave of sediment in the main river channels (right panel). This spatio-temporal analysis is crucial for understanding where in the network the greatest hazards (e.g., channel aggradation, impacts on water quality) might occur and how their location changes over time following an eruption.

5. Discussion

Our network-based stochastic case study serves as a "what-if" virtual testbed, providing a window into the complex, cascading interactions between volcanic and hydrological hazards. The results quantify these interactions and illustrate the potential value of this approach for Disaster Risk Management (DRM) within a complex multi-risk framework.

The primary contribution of this work is the conception and implementation of a functional virtual testbed for assessing cascading hazard impacts. The model can be used to test the sensitivity and long term dynamics of volcanic ash significantly altering catchment hydrology by reducing infiltration and increasing runoff — a significant risk for populations living downstream. Our testbed moves beyond static analysis by simulating the temporal evolution of this risk. The results explicitly visualize these cascading effects,

with the stock-and-flow analysis (Fig. 10) quantifying the mobilization and eventual depletion of ash stocks, while the hydrograph comparison (Fig. 11) provides quantitative evidence of increased flood peaks post-eruption. The simulation reveals that the period of heightened flood vulnerability can persist for months to years.

A key objective of virtual testbeds is to support decision-making under uncertainty. Our model achieves this through its stochastic hazard components and computationally efficient design, which enables the systematic exploration of "what-if" scenarios. The testbed allows risk managers to explore low-probability, high-impact events that are absent from historical records but pose a credible threat. By generating probabilistic outputs, the model helps decision-makers move beyond single, deterministic forecasts and instead allows them to assess the full range of potential outcomes, aiding in the effective allocation of resources to build more resilient communities.

It is important to acknowledge the model's design trade-offs. To achieve the computational efficiency required for rapid, stochastic, multi-year simulations, our model simplifies certain complex processes. For example, it treats ash as a single-class sediment and uses a simplified routing scheme. This distinction highlights a key strength of our model: it is purposefully designed as a streamlined and "light data requirement" simulation for focusing specifically on multihazard environments without accessible datasets. The model can easily incorporate additional data through the hazard and routing input modules.

While in some situations more complex models may produce more accurate outputs, this is not always the case for natural hazards [54] and is highly unlikely to be the case for multihazard models where a major limitation remains the lack of relevant data. When adding finer detail into a model, there comes a point where a new term serves no purpose because its effect is swamped under the uncertainty of the more major terms, and consequently contributes no real improvement to the model. This problem is amplified when including dynamic cascading interactions [22]. Thus, the focus here, and in the wider field, is on stochastic models that can aid both in decision-making for downstream effects, and also provide much needed insight into the complex interactions of different system components.

This streamlined, network-based architecture makes our virtual testbed a suitable "building block" for a larger, interconnected digital ecosystem of multi-risk models. Different models, with varying levels of complexity, can serve different but complementary roles. This work serves as a practical example of how a standalone testbed can be developed with the principles of interoperability and scalability, contributing a specific and crucial capability to a broader suite of tools for managing complex risks.

Scalability (from area to region to country) is straight-forward due to the bottom-up, compartmentalized structure of the methodology. All that is required is the addition of relevant nodes, using a stochastic model of choice and/or location of interest, and then define the connections between these (i.e., the edges). Examples of increasing model complexity are illustrated below in Section 5.1 through additional hazards (earthquakes, landslides), and critical infrastructure (stop-banks, man-made dams). Standardized input–output formats between nodes enable straightforward coupling with other hazard or impact models such as landslide or debris-flow simulations. In theory, any existing hazard model (or at least the output from it) can be made interoperable with this network model, but to realize the true potential of the virtual testbed these should be stochastic in nature, in order to sufficiently translate upstream to downstream uncertainties.

5.1. Additional stochastic hazard models

In order to fully simulate a multihazard scenario as illustrated in Fig. 3, we require phenomenological models for the remaining hazards listed in Table 2. Some possibilities are discussed below.

Regional earthquakes of magnitude 4 and up could be simulated using a Poisson process based on declustered [55] events from the NZ Earthquake catalogue (http://wfs.geonet.org.nz/). The magnitude of the simulated events is assumed to have a truncated exponential distribution on the interval $(4, 8)$ which satisfies the Gutenberg–Richter relationship on this interval. Large events have the potential to trigger damaging aftershocks, and these aftershocks are simulated using a bivariate Gaussian distribution centred on the parent, with an Omori decay in time [56]. Earthquake magnitude and epicentre is sent to each Landslide node in order to determine individual Landslide initiation probabilities. We can use existing models [57–59] to calculate Peak Ground Acceleration (PGA) at nodes of interest (Infrastructure, Natural Dam, and River Segment/Man-made Dam. As most earthquakes in New Zealand have occurred on previously unknown faults [60,61], we assume that all fault characteristics are the same within the region for GEM purposes.

Volcano-tectonic earthquakes can be omitted because the effects are considered negligible due to the limited magnitude [62] and considerable distance to any infrastructure, which are deemed earthquake resistant for such magnitudes. If included they would be a separate node, tied to the respective volcano, and with different spatial and impact links to those of the regional earthquake node.

An inundation flood requires the breach or overtopping of a stop bank along the river. Each River Segment/Man-made Dam and any Natural Dam nodes are connected to two Stop-bank nodes, one on each side of the river. The likelihood of a breach from the stop bank to the inundation area is a function of the water level above the stop bank divided by the height of the stop bank [63]. In the event of a breach, propagation from the respective River Segment/Man-made Dam or Natural Dam is assumed to occur instantaneously. A breach also dynamically reduces the stopbank height [64], with the water levels at the River Segment/Man-made Dam or Natural Dam reduced to this height. Note that if the water levels continue at this level, the Stop-bank will continue to fail until its height reaches that of the surrounding terrain.

Debris avalanches due to dome collapse at the Volcano may affect Infrastructure or River Segment/Man-made Dam nodes through a process that involves dome growth, collapse and subsequent flow. The destructiveness of debris avalanche flows mean that the intensity variable for debris avalanches at Infrastructure nodes is a binary variable indicating whether the debris avalanche arrives

at the location or not. Arrival at any single node is primarily controlled by the volume of the source avalanche [65]. Temporal occurrence is controlled by a Poisson process with parameters based on the work of Mendoza-Rosas et al. [66], which is reset by the explosion process above as an explosion will at least partially destroy the dome. The avalanche volume is function of the length of the growth period since the last collapse or explosion, and a random variable for the proportion of a dome mobilized in a collapse [67].

Landslides are only considered at locations where a) the slope exceeds some minimum amount and, b) to where a landslide could impact an Infrastructure node, or form a Natural Dam by infilling a River Segment/Man-made Dam. The probability of a Landslide being initiated could be parameterized as a simplified version of the model presented by Frigerio Porta et al. [68], where both rainfall (short- and long-term) and earthquake shaking contribute to the likelihood. Once a Landslide is initiated, it is propagated or not using the relationship from [13], where propagation occurs if the volume/run out is great enough compared to the 'distance' to the downstream node. Where a Landslide reaches an Infrastructure node, damage is assumed to be complete, however, where a Landslide reaches a River Segment / Man-made Dam, a sufficient volume is required to create a Natural Dam.

Once a Natural Dam exists, water and sediment are unable to propagate past and instead build up behind the Natural Dam until either dam failure or overtopping occurs. Dam failure could be modelled using a simplified form of the model from Frigerio Porta et al. [69], based on the water level, and the height and length of the natural dam. These values are inherited from the streamflow model, the Landslide volume that reached the original River Segment/Man-made Dam node, and the cross-section of the River Segment/Man-made Dam at that point. Should the Natural Dam fail, then propagation in the form of a lahar occurs at the next time step. The initial lahar volume is the accumulated water at the Natural Dam, plus that of the accumulated sediment at the Natural Dam. Lahars triggered from dam failure are typically catastrophic, causing flooding and geomorphic change downstream of the outbreak [70], such as from the 1315 Tarawera outbreak [9]. As a simplification to this process, all downstream nodes (including all River Segment/Man-made Dam, Stop-bank, and Infrastructure nodes) are considered destroyed/flooded, with the mass spread evenly across all downstream nodes. Alternatively, if the water height reaches the height of the dam, and the Natural Dam has not yet failed, water is allowed to propagate downstream over the Natural Dam; it becomes a weir.

5.2. A future for multihazard risk management

There is a need for models that can quantify multihazard occurrences and impacts, which can either increase [71,72] or decrease [73] risk. These considerations are particularly vital when applied to critical infrastructure [74,75]. Hazards can interact in many and complex ways, through triggering, coincidence and heightened likelihood [21,76–78]. Initial attempts to statistically correlate the risks and sidestep modelling hazard occurrence [79,80] have not been widely adopted, as they are limited to insurance applications. Many papers have outlined frameworks for assessment and management of multihazard risk [20,23,81–84], but the issue of parameterizing and quantifying occurrences, lags and magnitudes is greatly hampered by the absence of observed data at an appropriate resolution. While efforts have been made to assemble global datasets [85] for global analyses [86], regional or sub-regional data is almost unknown, forcing resort to expert judgement and elicitation [82]. These frameworks can also lack full spatio-temporal dimensionality, concentrating on scenario-based effects between event-defined hazard locations [23,87]. There is a clear need to develop quantified models with spatio-temporal resolution, which can then be used for risk analysis and consequent decision making [74,83,84].

In this paper we have taken a 'bottom-up' approach by piecing together a regional-scale simulation model for multihazard occurrences and impacts. To do so, we have leveraged simple, but sufficiently complex for this experiment, stochastic models for individual hazards, and linked these in a network structure. Physics-based simulations have been suggested by Jenkins et al. [88], but the computational demands will inevitably compromise the quantification of uncertainty in the results, as either scenarios must be resorted to, or very few simulations be performed. Accounting for every square meter of space is also computationally burdensome, and so we abstract space to only the locations that matter, either in terms of a cascading hazard, or a possible impact. A similar pragmatic approach to appropriate levels of detail has been suggested by Zuccaro et al. [89].

6. Conclusions

This study details the conceptualization and implementation of a dynamic, network-based virtual testbed for assessing cascading risks between volcanic ashfall and hydrological systems. By incorporating dynamic temporal processes within a computationally efficient framework, our model provides a realistic simulation environment for exploring multihazard interactions and their implications for Disaster Risk Management (DRM).

Our case-study application to the Rangitaiki and Tarawera river systems demonstrates that the testbed can effectively quantify the significant increase in flood risk caused by volcanic ashfall, particularly when compounded with high-intensity precipitation. The ability to run numerous "what-if" scenarios within a stochastic framework provides decision-makers with tools for planning under uncertainty.

This work serves as a proof-of-concept for how a virtual testbed can be designed as a modular, transferable building block. By making deliberate trade-offs between physical complexity and computational speed, it offers a promising pathway for bridging the gap between intensive research models and the practical, operational tools needed to help society navigate the challenges of complex, cascading disasters.

CRediT authorship contribution statement

Mark Bebbington: Writing – review & editing, Writing – original draft, Methodology, Investigation, Funding acquisition, Formal analysis, Conceptualization. **Alexandre Dunant:** Writing – review & editing, Writing – original draft, Visualization, Validation, Software, Methodology, Investigation, Formal analysis, Data curation, Conceptualization. **David Harte:** Writing – review & editing, Writing – original draft, Methodology, Investigation, Conceptualization. **Stuart Mead:** Writing – review & editing, Writing – original draft, Visualization, Methodology, Investigation, Funding acquisition, Formal analysis, Data curation, Conceptualization. **Melody Whitehead:** Writing – review & editing, Writing – original draft, Visualization, Methodology, Investigation, Funding acquisition, Data curation, Conceptualization.

Funding sources

This research was supported by the Resilience to Nature's Challenges Multihazard Risk programme, New Zealand (Grant number RNC-043) and the Endeavour Programme Te Awe Mapara, New Zealand (Grant number MAU2444), both funded by the New Zealand Ministry of Business, Innovation and Employment.

Declaration of competing interest

The authors declare the following financial interests/personal relationships which may be considered as potential competing interests: Mark Bebbington reports financial support and travel were provided by Ministry of Business Innovation and Employment. If there are other authors, they declare that they have no known competing financial interests or personal relationships that could have appeared to influence the work reported in this paper.

Appendix. Model equations and parameters

Here we provide more details of the governing equations used in the virtual testbed example.

A.1. Volcanic ashfall model

When an eruption is triggered, its magnitude, represented by the total erupted mass M_0, is drawn from a log-normal distribution:

$$M_0 = 10^{10.36+0.3Z} \tag{8}$$

[90], where Z is a standard normal random variable, $\mathcal{N}(0,1)$. This mass scales the parameters of the tephra fall model, which calculates the ash thickness, T (in cm), at a distance d (km) and angle θ (radians) from the vent:

$$T(d,\theta) = \gamma_{\text{eff}} \cdot \exp[-\beta U d(1-\cos(\theta-\phi))] \cdot d^{-\alpha_{\text{eff}}} \tag{9}$$

The parameters for this equation are determined stochastically for each eruption, using the following empirical relationships derived from simulating multiphase eruptions [91] using Tephra2 [92] to model the resulting ash dispersal:

- The effective eruption size, γ_{eff}, is scaled by the erupted mass and a baseline coefficient, γ_0:

$$\gamma_{\text{eff}} = \gamma_0 \cdot M_0^{0.46} \cdot 10^{0.11 Z_\gamma} \tag{10}$$

- The effective distance-decay exponent, α_{eff}, is inversely related to magnitude and controlled by a baseline coefficient, α_0:

$$\alpha_{\text{eff}} = \alpha_0 \cdot M_0^{-0.25} \cdot 10^{0.07 Z_\alpha} \tag{11}$$

- The main dispersal axis, ϕ, is determined by drawing a value $B \sim \text{Beta}(0.358, 0.317)$ and setting $\phi = 2\pi B$.
- A parameter controlling deposit elongation, βU, is derived from the decay exponent and a random component:

$$\beta U = 0.22 - 0.085\alpha_{\text{eff}} + 0.11 Z_{\beta U} \tag{12}$$

  The value of βU is redrawn if it becomes negative.

In the above equations, Z_γ, Z_α, and $Z_{\beta U}$ are independent standard normal random variables.

A.2. Hydrological response and ash transport

A.2.1. SCS-CN runoff calculation

The potential maximum soil moisture retention, S (in inches), is calculated from a baseline Curve Number (CN_{base}):

$$S_{\text{base}} = \frac{1000}{\text{CN}_{\text{base}}} - 10 \tag{13}$$

Initial abstraction, I_a, is modelled as a fraction (λ) of S:

$$I_a = \lambda S \tag{14}$$

The dynamic impact of ashfall is represented by an increase in the effective Curve Number (CN_{eff}). The increase, Δ_{CN}, follows an exponential saturation function based on ash thickness, h_{ash} (in mm), a maximum increase parameter, $\text{CN}_{\text{max\_increase}}$, and a decay constant, k_{ash}:

$$\Delta_{\text{CN}} = \text{CN}_{\text{max\_increase}} \left(1 - e^{-k_{\text{ash}} \cdot h_{\text{ash}}}\right) \tag{15}$$

$$\text{CN}_{\text{eff}} = \min(98, \text{CN}_{\text{base}} + \Delta_{\text{CN}}) \tag{16}$$

The final runoff depth, Q_{runoff} (in mm), for an hourly precipitation event, P (in mm), is calculated using the effective retention, S_{eff} (derived from CN_{eff}):

$$Q_{\text{runoff}} = \frac{(P - I_a)^2}{P - I_a + S_{\text{eff}}} \quad \text{for } P > I_a \tag{17}$$

A.2.2. Unit hydrograph generation

The catchment's time of concentration, t_c (in hours), is calculated using the Giandotti formula:

$$t_c = \frac{4\sqrt{A} + 1.5L}{0.8\sqrt{H}} \tag{18}$$

where A is the catchment area (km^2), L is the main channel length (km), and H is the total elevation drop (m). From this, the triangular Unit Hydrograph parameters – time to peak (t_p), time base (t_b), and peak discharge per unit of runoff (q_p) – are derived:

$$t_p = 0.6 \cdot t_c \tag{19}$$

$$t_b = 2.67 \cdot t_p \tag{20}$$

$$q_p = \frac{0.208A}{t_p} \tag{21}$$

A.2.3. Hillslope wash model

The mass of ash washed into the river, M_{wash}, is driven by the incremental runoff, Q_{runoff}. The potential mass washed is a function of the total available mass on the hillslope, M_{avail}, a wash efficiency parameter, η_{wash}, and a reference runoff depth, ΔQ_{ref} (10 mm):

$$M_{\text{wash, pot}} = M_{\text{avail}} \cdot \eta_{\text{wash}} \cdot \left(\frac{Q_{\text{runoff}}}{\Delta Q_{\text{ref}}}\right). \tag{22}$$

The actual mass washed is limited by the total mass available:

$$M_{\text{wash}} = \min(M_{\text{avail}}, M_{\text{wash, pot}}). \tag{23}$$

A.2.4. In-stream sediment (Ash) transport

Transport capacity is governed by bed shear stress, τ, which is calculated for each reach:

$$\tau = \rho_w g R_h S_0 \tag{24}$$

where ρ_w is water density, g is gravity, R_h is the hydraulic radius (a function of discharge and channel width), and S_0 is the channel slope. The transport capacity, T_c (in kg per time step), is a power-law function of shear stress, scaled by a transport coefficient (k_t), channel width (W), and length (L):

$$T_c = k_t \cdot (\tau^{1.5}) \cdot W \cdot L. \tag{25}$$

Data availability

The model code and simulation configuration files used in this study are publicly available on GitHub.

References

[1] B. Liu, Y.L. Siu, G. Mitchell, Hazard interaction analysis for multihazard risk assessment: a systematic classification based on hazard-forming environment, Nat. Hazards Earth Syst. Sci. 16 (2) (2016) 629–642.

[2] D. Guha-Sapir, R. Below, P. Hoyois, EM-DAT: The CRED/OFDA International Disaster Database, Www Documentation, Centre for Research on the Epidemiology of Disasters, 2016, url:www.emdat.be.

[3] DesInventar, Sendai framework for disaster risk reduction, disaster information management system, UNDRR DesInventar sendai, 2023, Retrieved from www.desinventar.net/what_is.html..

[4] T.C. Pierson, J.J. Major, A. Amigo, H. Moreno, Acute sedimentation response to rainfall following the explosive phase of the 2008–2009 Eruption of Chaitén volcano, Chile, Bull. Volcanol. 75 (5) (2013) 723.

[5] I. Sianko, Z. Ozdemir, I. Hajirasoulia, K. Pilakoutas, A probabilistic liquefaction hazard analysis: Case studies from the Marmara region, Geotech. Geol. Eng. 43 (2025) 103, http://dx.doi.org/10.1007/s10706-024-03042-6.

[6] M. Hughes, M. Quigley, S. Van Ballegooy, B. Deam, B. Bradley, D. Hart, R. Measures, The sinking city: Earthquakes increase flood hazard in Christchurch, New Zealand, GSA Today 25 (3–4) (2015) 4–10, http://dx.doi.org/10.1130/GSATG221A.1.

[7] G. Barla, P. Paronuzzi, The 1963 vajont landslide: 50th anniversary, Rock Mech. Rock Eng. 46 (6) (2013) 1267–1270.

[8] S. Sahetapy-Engel, S. Self, R.J. Carey, I.A. Nairn, Deposition and generation of multiple widespread fall units from the c. AD 1314 Kaharoa rhyolitic eruption, Tarawera, New Zealand, Bull. Volcanol. 76 (2014) 1–28, http://dx.doi.org/10.1007/s00445-014-0836-4.

[9] K. Hodgson, I. Nairn, The c. AD 1315 syn-eruption and AD 1904 post-eruption breakout floods from Lake Tarawera, Haroharo Caldera, North Island, New Zealand, N. Z. J. Geol. Geophys. 48 (3) (2005) 491–506, http://dx.doi.org/10.1080/00288306.2005.9515128.

[10] K.B. Gran, D.R. Montgomery, .D.G. Sutherland, Channel bed evolution and sediment transport under declining sand inputs, Water Resour. Res. 42 (10) (2006) W10407.

[11] K.B. Gran, D.R. Montgomery, J.C. Halbur, Long-term elevated post-eruption sedimentation at Mount Pinatubo, Philippines, Geology 39 (4) (2011) 367–370.

[12] K. Ujjwal, S. Garg, J. Hilton, J. Aryal, A cloud-based framework for sensitivity analysis of natural hazard models, Environ. Model. Softw. 134 (2020) 104800, http://dx.doi.org/10.1016/j.envsoft.2020.104800.

[13] A. Dunant, M. Bebbington, T. Davies, Probabilistic cascading multihazard risk assessment methodology using graph theory, a New Zealand trial, Int. J. Disaster Risk Reduct. 54 (2021b) 102018.

[14] Z. Liu, F. Nadim, A. Garcia-Aristizabal, A. Mignan, K. Fleming, B. Luna, A three-level framework for multi-risk assessment, Georisk: Assess. Manag. Risk Eng. Syst. Geohazards 9 (2) (2015) 59–74, http://dx.doi.org/10.1080/17499518.2015.1041989.

[15] A. Mignan, S. Wiemer, D. Giardini, The quantification of low-probability-high-consequences events: Part I. A generic multi-risk approach, Nat. Hazards 73 (3) (2014) 1999–2022, http://dx.doi.org/10.1007/s11069-014-1178-4.

[16] S. Dellow, C. Massey, S. Cox, Response and initial risk management of landslide dams caused by the 14 november 2016 kaikoura earthquake, south island, new zealand, in: Proceedings of the 20th NZGS Geotechnical Symposium, Napier NZ, 2017a, pp. 400–407, URL: https://www.nzgs.org/libraries/proceedings-of-the-20th-nzgs-symposium/.

[17] S. Dellow, C. Massey, S. Cox, G. Archibald, J. Begg, Z. Bruce, J. Carey, J. Davidson, F.D. Pasqua, P. Glassey, M. Hill, K. Jones, B. Lyndsell, B. Lukovic, S. McColl, M. Rattenbury, S. Read, B. Rosser, C. Singeisen, D. Townsend, P. Villamor, M. Villeneuve, J. Godt, R. Jibson, K. Allstadt, F. Rengers, J. Wartman, E. Rathje, N. Sitar, A.-Z. Adda, J. Manousakis, M. Little, Landslides caused by the M_w 7.8 kaikōura earthquake and the immediate response, Bull. N. Z. Soc. Earthq. Eng. 50 (2) (2017b) 106–116, http://dx.doi.org/10.5459/bnzsee.50.2.106-116.

[18] R.W. Jibson, K.E. Allstadt, F.K. Rengers, J.W. Godt, Overview of the Geologic Effects of the November 14 2016, M_w 7.8 Kaikoura, New Zealand, Earthquake, U.S. Geological Survey Scientific Investigations Report 2017–5146, U.S. Geological Survey, Denver CO, 2018, http://dx.doi.org/10.3133/sir20175146.

[19] C. Park, H.-U. Schmincke, Multistage damming of the Rhine River by tephra fallout during the 12 900BP Plinian Laacher see Eruption (Germany), syn-eruptive Rhine damming I, J. Volcanol. Geotherm. Res. 389 (2020) 106688, http://dx.doi.org/10.1016/j.jvolgeores.2019.106688.

[20] M.S. Kappes, M. Keiler, K. von Elverfeldt, T. Glade, Challenges of analyzing multihazard risk: a review. natural hazards, Nat. Hazards 64 (2) (2012) 1925–1958, http://dx.doi.org/10.1007/s11069-012-0294-2.

[21] J.C. Gill, B.D. Malamud, Reviewing and visualizing the interactions of natural hazards, Rev. Geophys. 52 (4) (2014) 680–722.

[22] J.C. Gill, B.D. Malamud, Hazard interactions and interaction networks (cascades) within multihazard methodologies, Earth Syst. Dyn. 7 (3) (2016) 659–679, https://doi.org/10.5194/esd-7-659-2016.

[23] S.De. Angeli, B. Malamud, L. Rossi, F. Taylor, E. Trasforini, R. Rudari, A multihazard framework for spatial–temporal impact analysis, Int. J. Disaster Risk Reduct. 73 (2022) 102829.

[24] A. Dunant, Are we missing the target? A bias–variance perspective on multihazard risk assessment, Front. Earth Sci. 9 (2021) 685301, http://dx.doi.org/10.3389/feart.2021.685301.

[25] A. Dunant, M. Bebbington, T. Davies, P. Horton, Multihazards scenario generator: A network-based simulation of natural disasters, Risk Anal. 41 (11) (2021a) 2154–2176.

[26] I.A. Nairn, Geology of the Okataina Volcanic Centre, Scale 1:50 000, Institute of Geological & Nuclear Sciences geological map 25, 2002.

[27] P.R. Chappell, The Climate and Weather of the Bay of Plenty, third ed., NIWA, 2013, p. 40.

[28] E. Smith, C. Oppenheimer, The edgecumbe earthquake sequence: 1987 February to March 18, N. Z. J. Geol. Geophys. 32 (1) (1989) 31–42, http://dx.doi.org/10.1080/00288306.1989.10421386.

[29] A. Simon, Post-Earthquake Response of the Lower Rangitaiki River, Technical report, Cardno Limited, 2017, URL: nz.linkedin.com/company/cardno.

[30] T.M. Wilson, J.W. Cole, Potential impact of ash eruptions on dairy farms from a study of the effects on a farm in Eastern Bay of Plenty, New Zealand; implications for hazard mitigation, Nat. Hazards 43 (2007) 103–128, http://dx.doi.org/10.1007/s11069-007-9111-8.

[31] H. Craig, T. Wilson, C. Magill, C. Stewart, A. Wild, Agriculture and forestry impact assessment for tephra fall hazard: fragility function development and New Zealand scenario application, Volcanica 4 (2) (2021) 345–367, http://dx.doi.org/10.30909/vol.04.02.345367.

[32] T. Davies, S. Mead, M. Bebbington, A. Dunant, D. Grimson, G. Harmsworth, D. Harte, E. Harvey, R. Paulik, G. McDonald, N. Smith, M. Whitehead, Multihazard Risk Model, Flooding Case Study: Selection of River System and Potential Hazard Cascades, ME technical report, ME Research, Takapuna, 2020, URL: http://www.marketeconomics.co.nz/resilience-challenge/publications/selection-of-river-system-and-potential-hazard.

[33] J.A. Bondy, U.S.R. Murty, Graph Theory with Applications, North-Holland, New York, ISBN: 0-444-19451-7, 1976.

[34] N. Boccara, Modeling Complex Systems, Springer Nature, Switzerland, 2010, http://dx.doi.org/10.1007/978-1-4419-6562-2.

[35] C. Butts, Revisiting the foundations of network analysis, Science 325 (5939) (2009) 414–416, http://dx.doi.org/10.1126/science.1171022.

[36] J. Phillips, W. Schwanghart, T. Heckmann, Graph theory in the geosciences, Earth-Sci. Rev. 143 (2015) 147–160, http://dx.doi.org/10.1016/j.earscirev.2015.02.002.

[37] P. Holme, J. Saramäki, Temporal networks, Phys. Rep. 519 (3) (2012) 97–125, http://dx.doi.org/10.1016/j.physrep.2012.03.001.

[38] U. Scharler, S. Borrett, Network construction, evaluation and documentation: A guideline, Environ. Model. Softw. 140 (2021) 105020, http://dx.doi.org/10.1016/j.envsoft.2021.105020.

[39] V. Grimm, E. Revilla, U. Berger, F. Jeltsch, W. Mooij, S. Railsback, H.-H. Thulke, J. Weiner, T. Wiegand, D. DeAngelis, Pattern-oriented modeling of agent-based complex systems: Lessons from ecology, Science 310 (5750) (2005) 987–991, http://dx.doi.org/10.1126/science.1116681.

[40] S. Abe, N. Suzuki, Complex-network description of seismicity, Nonlinear Process. Geophys. 13 (2) (2006) 145–150, http://dx.doi.org/10.5194/npg-13-145-2006.

[41] D. Pastén, F. Torres, B. Toledo, V. Muñoz, J. Rogan, J. Valdivia, Time-based network analysis before and after the M_w 8.3 Illapel Earthquake 2015 Chile, Pure Appl. Geophys. 173 (7) (2016) 2267–2275, http://dx.doi.org/10.1007/s00024-016-1335-7.

[42] S. Robinson, Discrete-event simulation: From the pioneers to the present, what next? J. Oper. Res. Soc. 56 (2005) 619–629, http://dx.doi.org/10.1057/palgrave.jors.2601864.

[43] P.A.W. Lewis, G.S. Shedler, Simulation of non-homogeneous Poisson processes by thinning, Nav. Res. Logist. Q. 26 (1979) 403–413.

[44] Y. Ogata, On Lewis' simulation mehod for point processes, IEEE Trans. Inform. Theory 27 (1981) 23–31.

[45] L. Iannacone, K. Otarola, R. Gentile, G. Galasso, Simulating multi-hazard event sets for life cycle consequence analysis, Nat. Hazards Earth Syst. Sci. 24 (2024) 1721–1740.

[46] E.T. Coon, J.D. Moulton, S.L. Painter, Managing complexity in simulations of land surface and near-surface processes, Environ. Model. Softw. 78 (2016) 134–149, http://dx.doi.org/10.1016/j.envsoft.2015.12.017.

[47] R. Lowe, C. Urich, M. Kulahci, M. Radhakrishnan, A. Deletic, K. Arnbjerg-Nielsen, Simulating flood risk under non-stationary climate and urban development conditions – experimental setup for multiple hazards and a variety of scenarios, Environ. Model. Softw. 102 (2018) 155–171, http://dx.doi.org/10.1016/j.envsoft.2018.01.008.

[48] M. Bebbington, C. Lai, On nonhomogeneous models for volcanic eruptions, Mathemtical Geol. 28 (5) (1996) 585–600, http://dx.doi.org/10.1007/BF02066102.

[49] A.O. González-Mellado, S. De la Cruz-Reyna, A simple semi-empirical approach to model thickness of ash-deposits for different eruption scenarios, Nat. Hazards Earth Syst. Sci. 10 (11) (2010) 2241–2257, http://dx.doi.org/10.5194/nhess-10-2241-2010.

[50] U.S. Department of Agriculture, Soil Conservation Service, Urban hydrology for small watersheds (technical release 55), 1986.

[51] T.C. Pierson, J.J. Major, Hydrogeomorphic effects of explosive volcanic eruptions on drainage basins, Annu. Rev. Earth Planet. Sci. 42 (2014) 469–507.

[52] P.I.A. Kinnell, Event soil loss, runoff and the universal soil loss equation family of models: A review, J. Hydrol. 385 (2010) 384–397.

[53] R.E. Horton, Erosional development of streams and their drainage basins; hydrophysical approach to quantitative morphology, Geol. Soc. Am. Bull. 56 (3) (1945) 275–370.

[54] J.E.M. Baartman, L.A. Melsen, D. Moore, M.J. van der Ploeg, On the complexity of model complexity: Viewpoints across the geosciences, CATENA 186 (2020) 104261, http://dx.doi.org/10.1016/j.catena.2019.104261.

[55] J. Gardner, L. Knopoff, Is the sequence of earthquakes in southern california, with aftershocks removed, Poissonian? Bull. Seismol. Soc. Am. 64 (5) (1974) 1363–1367, http://dx.doi.org/10.1785/bssa0640051363.

[56] D. Harte, Bias in fitting the ETAS model: A case study based on New Zealand seismicity, Geophys. J. Int. 192 (1) (2013) 390–412, http://dx.doi.org/10.1093/gji/ggs026.

[57] GEM, OpenQuake-Engine Book: Risk V1.0.0, GEM Foundation, Pavia Italy, 2013.

[58] GEM, OpenQuake-Engine Book: Hazard V1.0.0, GEM Foundation, Pavia Italy, 2014.

[59] GEM, The OpenQuake-Engine User Manual V3.14.0, GEM Foundation, Pavia Italy, 2022.

[60] M. Stirling, G. McVerry, M. Gerstenberger, N. Litchfield, R.Van. Dissen, K. Berryman, P. Barnes, L. Wallace, P. Villamor, R. Langridge, G. Lamarche, S. Nodder, M. Reyners, B. Bradley, D. Rhoades, W. Smith, A. Nicol, J. Pettinga, K. Clark, K. Jacobs, National seismic hazard model for New Zealand: 2010 update, Bull. Seismol. Soc. Am. 102 (4) (2012) 1514–1542, http://dx.doi.org/10.1785/0120110170.

[61] D. Harte, Evaluation of earthquake stochastic models based on their real-time forecasts: A case study of Kaikoura 2016, Geophys. J. Int. 217 (3) (2019) 1894–1914, http://dx.doi.org/10.1093/gji/ggz088.

[62] J. Mori, R. White, D. Harlow, P. Okubo, J. Power, R. Hoblitt, E. Laguerta, A. Lanuza, B. Bautista, Volcanic earthquakes following the 1991 climatic eruption of mount pinatubo: strong seismicity during a waning eruption, in: C. Newhall, R. Punongbayan (Eds.), Fire and Mud: Eruptions and Lahars of Mount Pinatubo, Phillipines, University of Washington Press, Seattle, 1995.

[63] N.P.L. Acosta, J.R.C. Tutivén, D.F.B. Galdámez, M.Á.J. Téllez, C. Zwanenburg, Obtaining fragility curves on levees subjected to flooding, in: Proceedings of the XVII ECSMGE-2019, Geotechnical Engineering Foundation of the Future, 2019, URL: https://www.ecsmge-2019.com/.

[64] J. Danka, L.M. Zhang, Dike failure mechanisms and breaching parameters, J. Geotech. Geoenvironmental Eng. 141 (9) (2015) 04015039, http://dx.doi.org/10.1061/(ASCE)GT.1943-5606.0001335.

[65] S.R. Mead, J. Procter, M. Bebbington, Probabilistic volcanic mass flow hazard assessment using statistical surrogates of deterministic simulations, Comput. Geosci. 178 (2023) 105417, http://dx.doi.org/10.1016/j.cageo.2023.105417.

[66] A.T. Mendoza-Rosas, Á. Gómez-Vázquez, S. De la Cruz-Reyna, Statistical analysis of the sustained lava dome emplacement and destruction processes at Popocatépetl Volcano, Central México, Bull. Volcanol. 79 (2017) 1–13, http://dx.doi.org/10.1007/s00445-017-1127-7.

[67] C.E. Harnett, M.E. Thomas, E.S. Calder, S.K. Ebmeier, A. Telford, W. Murphy, J. Neuberg, Presentation and analysis of a worldwide database for lava dome collapse events: the global archive of dome instabilities (GLADIS), Bull. Volcanol. 81 (2019) 1–17.

[68] G. Frigerio Porta, M. Bebbington, X. Xiao, G. Jones, A statistical model for earthquake and/or rainfall triggered landslides, Front. Earth Sci. 8 (2021) art605003, http://dx.doi.org/10.3389/feart.2020.605003.

[69] G. Frigerio Porta, M. Bebbington, G. Jones, X. Xiao, Bayesian lifetime analysis for landslide dams, Landslides 17 (8) (2020) 1835–1848, http://dx.doi.org/10.1007/s10346-020-01388-5.

[70] V. Manville, K.A. Hodgson, I.A. Nairn, A review of break-out floods from volcanogenic lakes in New Zealand, N. Z. J. Geol. Geophys. 50 (2) (2007) 131–150, http://dx.doi.org/10.1080/00288300709509826.

[71] K. Fleming, S. Parolai, A. Garcia-Aristizabal, S. Tyagunov, S. Vorogushyn, H. Kreibich, H. Mahlke, Harmonizing and comparing single-type natural hazard risk estimations, Ann. Geophysics 59 (2) (2016) 1–9, http://dx.doi.org/10.4401/ag-6987.

[72] J. Zhang, Y. Bagtzoglou, J. Zhu, B. Li, W. Zhang, Fragility-based system performance assessment of critical power infrastructure, Reliab. Eng. Syst. Saf. 232 (2023a) 109065, http://dx.doi.org/10.1016/j.ress.2022.109065.

[73] J. Hillier, T. Matthews, R. Wilby, C. Murphy, Multihazard dependencies can increase or decrease risk, Nat. Clim. Chang. 10 (7) (2020) 595–598, http://dx.doi.org/10.1038/s41558-020-0832-y.

[74] E. Choi, J.-G. Ha, D. Hahm, M. Kim, A review of multihazard risk assessment: Progress, potential, and challenges in the application to nuclear power plants, Int. J. Disaster Risk Reduct. 53 (2021) 101933, http://dx.doi.org/10.1016/j.ijdrr.2020.101933.

[75] Y. Cheng, E. Elsayed, X. Chen, Random multi hazard resilience modeling of engineered systems and critical infrastructure, Reliab. Eng. Syst. Saf. 209 (2021) 107453, http://dx.doi.org/10.1016/j.ress.2021.107453.

[76] M. Kumasaki, M. King, M. Arai, L. Yang, Anatomy of cascading natural disasters in Japan: Main modes and linkages, Nat. Hazards 80 (3) (2016) 1425–1441, http://dx.doi.org/10.1007/s11069-015-2028-8.

[77] A. Tilloy, B. Malamud, H. Winter, A. Joly-Laugel, A review of quantification methodologies for multihazard interrelationships, Earth-Sci. Rev. 196 (2019) 102881, http://dx.doi.org/10.1016/j.earscirev.2019.102881.

[78] J. Wang, Z. He, W. Weng, A review of the research into the relations between hazards in multihazard risk analysis, Nat. Hazards 104 (3) (2020) 2003–2026, http://dx.doi.org/10.1007/s11069-020-04259-3.

[79] W. Marzocchi, A. Garcia-Aristizabal, P. Gasparini, M. Mastellone, A. Di Ruocco, Basic principles of multi-risk assessment: A case study in Italy, Nat. Hazards 62 (2) (2012) 551–573, http://dx.doi.org/10.1007/s11069-012-0092-x.

[80] J. and Selva, Long-term multi-risk assessment: Statistical treatment of interaction among risks, Nat. Hazards 67 (2) (2013) 701–722, http://dx.doi.org/10.1007/s11069-013-0599-9.
[81] N. Komendantova, A. Scolobig, A. Garcia-Aristizabal, D. Monfort, K. Fleming, Multi-risk approach and urban resilience, Int. J. Disaster Resil. Built Environ. 7 (2) (2016) 114–132, http://dx.doi.org/10.1108/IJDRBE-03-2015-0013.
[82] J. Gill, B. Malamud, E. Barillas, A. Noriega, Construction of regional multihazard interaction frameworks, with an application to guatemala, Nat. Hazards Earth Syst. Sci. 20 (1) (2020) 149–180, http://dx.doi.org/10.5194/nhess-20-149-2020.
[83] S. Hochrainer-Stigler, R. Trogrlić Šakić, K. Reiter, P. Ward, M. de Ruiter, M. Duncan, S. Torresan, R. Ciurean, J. Mysiak, D. Stuparu, S. Gottardo, Toward a framework for systemic multihazard and multi-risk assessment and management, IScience 26 (5) (2023) 106736, http://dx.doi.org/10.1016/j.isci.2023.106736.
[84] S. Zhang, B. Wang, L. Zhang, S. Lacasse, F. Nadim, Y. Chen, Increased human risk caused by cascading hazards – a framework, Sci. Total Environ. 857 (2023b) 159308, http://dx.doi.org/10.1016/j.scitotenv.2022.159308.
[85] J. Claassen, P. Ward, J. Daniell, E. Koks, T. Tiggeloven, M. de Ruiter, A new method to compile global multihazard event sets, Sci. Rep. 13 (1) (2023) 13808, http://dx.doi.org/10.1038/s41598-023-40400-5.
[86] P. Ward, V. Blauhut, N. Bloemendaal, E. Daniell, C.De. Ruiter, J. Duncan, R. Emberson, F. Jenkins, D. Kirschbaum, M. Kunz, S. Mohr, S. Muis, A. Riddell, A. Schäfer, T. Stanley, I. Veldkamp, C. Winsemius, Review article: Natural hazard risk assessments at the global scale, Nat. Hazards Earth Syst. Sci. 20 (4) (2020) 1069–1096, http://dx.doi.org/10.5194/nhess-20-1069-2020.
[87] M. Zharikova, V. Sherstjuk, Event-based spatially-distributed multihazard risk analysis, in: 2020 IEEE 15th International Conference on Computer Sciences and Information Technologies, CSIT, vol. 2, 2020, pp. 273–276, http://dx.doi.org/10.1109/CSIT49958.2020.9321990.
[88] L. Jenkins, M. Creed, K. Tarbali, M. Muthusamy, R. Trogrlić, J. Phillips, C. Watson, H. Sinclair, C. Galasso, J. McCloskey, Physics-based simulations of multiple natural hazards for risk-sensitive planning and decision-making in expanding urban regions, Int. J. Disaster Risk Reduct. 84 (2023) 103338, http://dx.doi.org/10.1016/j.ijdrr.2022.103338.
[89] G. Zuccaro, D. De Gregorio, M. Leone, Theoretical model for cascading effects analyses, Int. J. Disaster Risk Reduct. 30 (2018) 199–215, http://dx.doi.org/10.1016/j.ijdrr.2018.04.019.
[90] L. Mastin, M. Guffanti, R. Servranckx, P. Webley, S. Barsotti, K. Dean, A. Durant, J. Ewert, A. Neri, W. Rose, D. Schneider, L. Siebert, B. Stunder, G. Swanson, A. Tupper, A. Volentik, C. Waythomas, A multidisciplinary effort to assign realistic source parameters to models of volcanic ash-cloud transport and dispersion during eruptions, J. Volcanol. Geotherm. Res. 186 (1–2) (2009) 10–21, http://dx.doi.org/10.1016/j.jvolgeores.2009.01.008.
[91] M.S. Bebbington, S.F. Jenkins, Intra-eruption forecasting using analogue volcano and eruption sets, J. Geophys. Res. 127 (2022) e2022JB024343.
[92] C. Bonadonna, C.B. Connor, B.F. Houghton, L. Connor, M. Byrne, A. Laing, T.K. Hincks, Probabilistic modeling of tephra dispersal: Hazard assessment of a multiphase Rhyolitic Eruption at tarawera, New Zealand, J. Geophys. Res. 110 (2005) B03203.